Dynamical properties of the normal phase of betaine calcium chloride dihydrate. I. Experimental results

1996 J. Phys.: Condens. Matter 8 8207

(http://iopscience.iop.org/0953-8984/8/43/016)

J. Phys.: Condens. Matter **8** (1996) 8207–8219. Printed in the UK

Dynamical properties of the normal phase of betaine calcium chloride dihydrate. I. Experimental results

J Hlinka†, M Quilichini†, R Currat‡ and J F Legrand‡

† Laboratoire Léon Brillouin, Centre d'Etudes de Saclay, Gif-sur-Yvette, France
‡ Institute Laue–Langevin, 38042 Grenoble, France

Received 23 April 1996, in final form 10 July 1996

Abstract. Coherent inelastic neutron scattering results obtained at different temperatures in the normal phase of betaine calcium chloride dihydrate (BCCD) are reported here. The experimental characterization of the mechanism which induces the transition from the parent phase to the incommensurate phase of BCCD is described. We show that the three lower-energy phonon branches of symmetry Λ_3–Λ_2 are temperature sensitive; the lowest of the three displays a conspicuous softening at a wavevector $\boldsymbol{q} = 0.3c^*$ at $T = T_i = 164$ K. The present neutron scattering results are in good agreement with previous Raman and IR measurements.

1. Introduction

In the present paper we report neutron scattering studies on betaine calcium chloride dihydrate (BCCD) ($(CH_3)_3NCH_2COO.CaCl_2.2H_2O$). BCCD has been one of the most studied dielectric compounds over the last few years. Its phase diagram is a textbook example of a 'devil's staircase', with up to 17 modulated commensurate and incommensurate phases in the temperature range 165–45 K [1–3]. Under hydrostatic pressure [4, 5, 7], or under an applied electric field [6, 7], the number of modulated phases is further increased.

The normal or parent phase of BCCD, stable above $T_i = 164$ K, is orthorhombic. At atmospheric pressure and at $T_i = 164$ K there is a transition to a modulated incommensurate phase. Zuniga *et al* [8] have determined its superspace group as $P(Pnma)$:$(1, s, -1)$. The average structure has the same space group as the normal phase and the frozen static distortion has a wavevector $k = \delta(T)c^*$. When the temperature is lowered to $T_c = 115$ K in the incommensurate phase, the wavevector decreases smoothly. A commensurate ($\frac{2}{7}$) phase exists in the temperature range 125–127 K. Perez-Mato [9] has proposed a phenomenological analysis, in the framework of Landau theory, based on the assumption of only one order parameter inducing the complete sequence of phase transitions. Then, the superspace group proposed by Zuniga *et al* [8] to describe the structure of the incommensurate phase gives the symmetry of the order parameter and of the various commensurate phases.

Our experimental work was undertaken to complement previous results obtained by Currat *et al* [10]. The sample used in the present work was fully deuterated in order to eliminate the large incoherent cross section from the hydrogen atoms. The format of the present paper is as follows. In section 2, we present a structural description of the normal phase of BCCD and the symmetry properties related to it. In section 3 we describe the experimental set-up while in section 4 we present and discuss the experimental results obtained in the normal phase at four different temperatures.

0953-8984/96/438207+13$19.50

2. Structural and symmetry properties of the room-temperature phase of BCCD

The normal phase crystallizes with space group $Pnma$, with $a = 10.97$ Å, $b = 10.15$ Å and $c = 10.82$ Å. It has four formula units per primitive cell, as first established by Brill *et al* [11]. The formula unit shown in figure 1 consists of two entities which have the same m site symmetry.

(i) *The betaine molecule.* This inner salt of trimethyl aminoacetic acid is a zwitterionic (dipolar) molecule. The positive charge is located on the nitrogen (N) atom while the negative charge is on the carboxyl group C(4)–O(1)O(2).

(ii) *The 'Ca' complex.* The environment of the Ca^{2+} ion consists of two Cl^- ions and two water molecules. Furthermore this 'Ca' inorganic complex is connected to two different neighbouring betaine molecules by the oxygen atoms O(1) and O(2) of the carboxyl groups of the betaine.

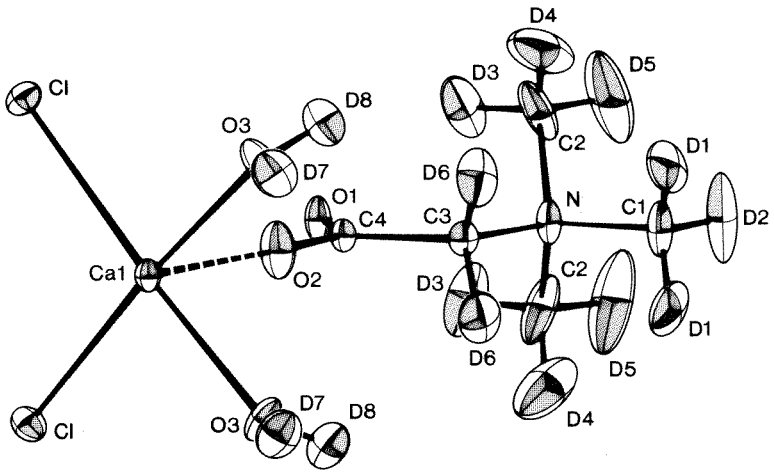

Figure 1. The formula unit of BCCD. The two entities defined in the text are represented. The atoms are labelled after the notation of Brill *et al* [11]. Ca, C(4), O(1), O(2), C(3), N, C(1), D(2) atoms belong to a mirror plane m. The thermal ellipsoids have been obtained from refinements of neutron diffraction data at 300 K and in the present figure they are reduced to 10% of their real value [14].

In the m mirror planes of the $Pnma$ structure, the BCCD formula units form zigzag chains along the a direction. The structure can be viewed as a series of sheets normal to the b axis which coincide with the m mirror planes located at $y = \frac{1}{4}b$ and $y = \frac{3}{4}b$, respectively.

These sheets are connected by a net of hydrogen bridges (Cl–H–O(3)) between the inorganic 'Ca complexes' as can be seen in figure 2. This system of H bonds is rather different from that observed either in betaine arsenate [13] or in betaine phosphate [12], where molecular motions are hindered by H bonding between organic and inorganic components.

In the structural work of Brill *et al* [11] it was shown also that the two entities (betaine and the 'Ca' complex) execute large librational motions around axes which belong to the m planes. More specifically, figure 3 shows on one m plane the axes of libration of the deuterated betaine, obtained from our neutron diffraction data [14], together with the

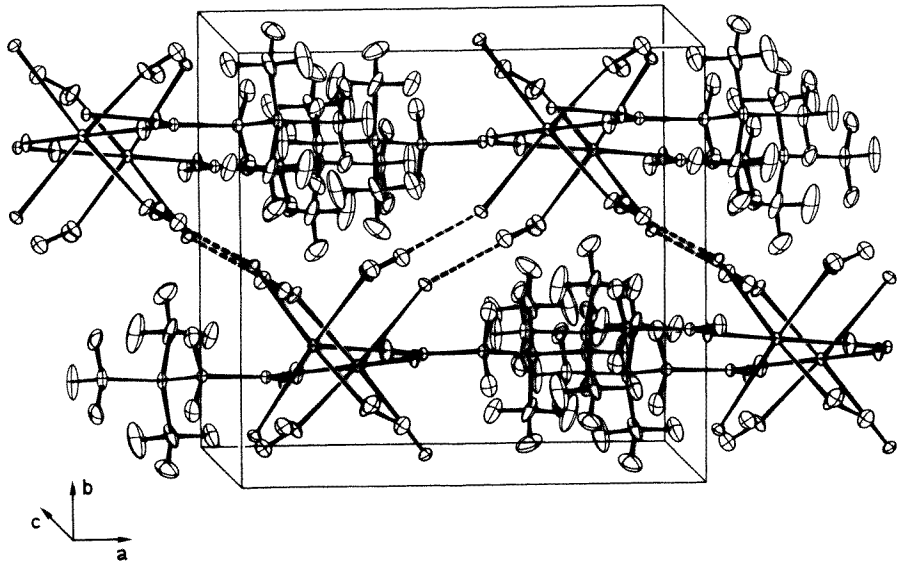

Figure 2. The unit cell of BCCD. Deuterium bridges Cl–H–O(3) are clearly seen in planes (011) and (0$\bar{1}$1). Thermal ellipsoids (obtained from neutron diffraction data [14]) have been reduced to 10% of their true value.

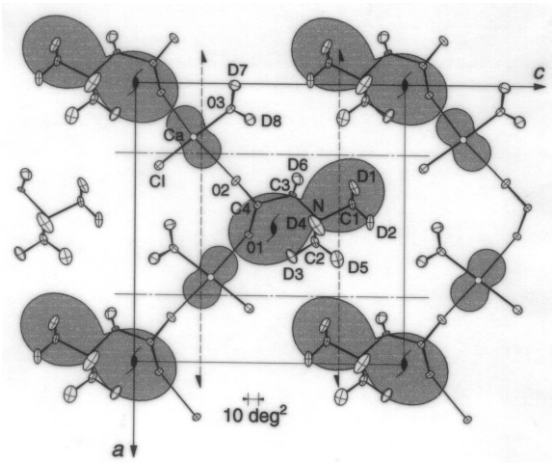

Figure 3. Projection on the *m* plane of the polar diagrams of the betaine molecules, obtained from neutron diffraction data [14]. The polar diagram (in degrees squared) for the betaine molecules indicate the direction of the main axis of libration. This axis is nearly the same as, that proposed by Brill *et al* [11]. The polar diagrams for the 'Ca' complexes are taken from Brill *et al* [11].

libration axes for the 'Ca' complexes. Note that the amplitudes of motion of the betaine molecules are much larger than those of the 'Ca' complexes. In the context of Raman data, Dvořàk [15] has discussed the symmetry properties of these motions. In the site, they have an A′ symmetry which induces normal modes belonging to the B_{1g}, B_{3g}, B_{2u} and A_u irreducible representations of the factor group of the crystal. Table 1 summarizes the symmetry correlations for modes propagating along either c^* or a^*.

Table 1. Symmetry correlations. T_a, T_b and T_c refer to translations parallel to a, b and c axes, respectively, and R_a, R_b and R_c refer to rotations about a, b and c axes, respectively.

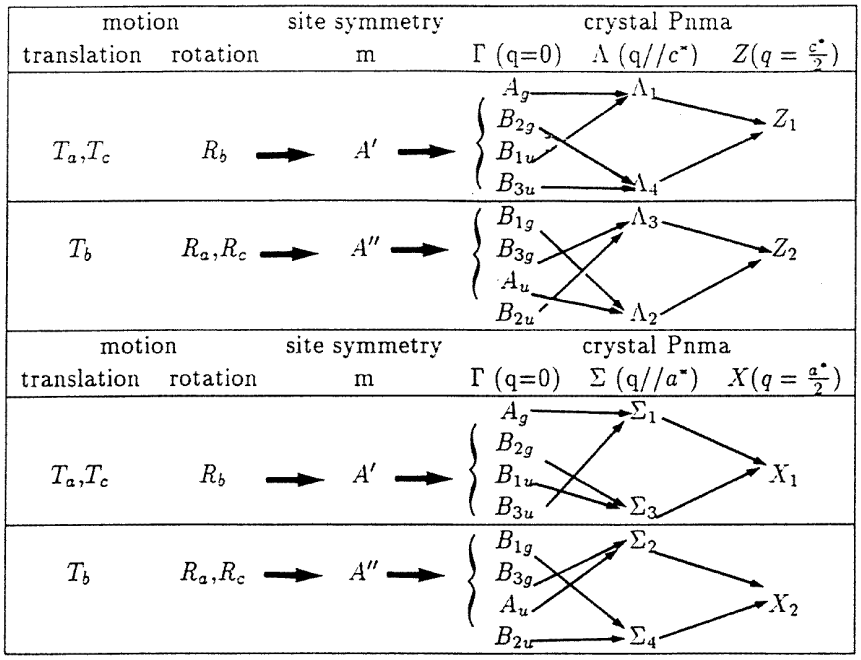

Finally from the symmetry of the incommensurate phase, it is clear that the order parameter belongs to the Λ_3 irreducible representation of $Pnma$.

3. Experimental details

3.1. The sample

A large single crystal (about 2 cm^3) of BCCD, with natural faces parallel to (011) and $(0\bar{1}1)$, has been grown by slow evaporation from a saturated D_2O solution of totally deuterated chemicals by J M Godard, Laboratoire de Physique des Solides, Université de Paris-Sud, Orsay. The crystal, enclosed in an aluminium container, was mounted on the cold finger of a Displex closed-cycle cryostat. The temperature stability was 0.2 K. All measurements were performed on the 4F three-axis spectrometers located on a cold source at the Orphée Reactor at Centre d'Etudes de Saclay (France).

3.2. The scattering plane

In a three-axis experiment, this plane is defined by the wavevectors $\boldsymbol{k}_i$ and $\boldsymbol{k}_f$ of the incoming and outgoing neutron beam, respectively. The momentum transfer $\boldsymbol{H}$ is given by

$$\boldsymbol{k}_i - \boldsymbol{k}_f = \boldsymbol{H} = \boldsymbol{G} + \boldsymbol{q} \tag{3.1}$$

where $\boldsymbol{q}$ is the wavevector of the excitation measured from the Brillouin zone centre defined by the the reciprocal-lattice vector $\boldsymbol{G}$. We have worked in two different planes.

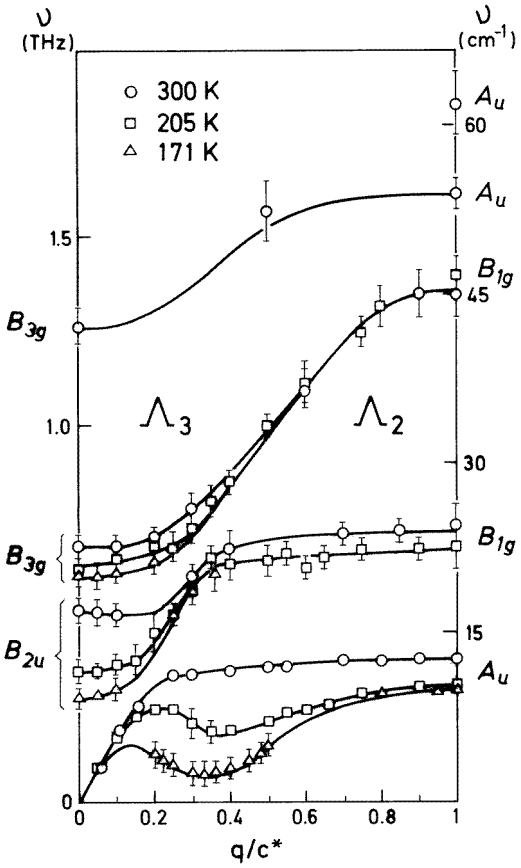

Figure 4. Dispersion curves of low-energy Λ_2–Λ_3 modes, at three temperatures. The full curves are guides for the eye. The different symbols are explained in the text.

(a) *The b^*–c^* plane.* In this plane, one can measure modes propagating along the c^* direction which belong to the Λ_3 and Λ_2 symmetries and are mainly transverse, polarized along b. At the Brillouin zone boundary Z ($q = c^*/2$) the pair Λ_3–Λ_2 is degenerate and thus it is convenient to display dispersion curves in the *extended Brillouin zone scheme* where one pair Λ_3–Λ_2 gives a single curve (see figure 4). Moreover, the one-phonon inelastic structure factor of the modes follows an intensity pattern consistent with this scheme, making symmetry assignment of the measured phonons straightforward. In this scattering plane the Brillouin zones investigated are those centred at the Bragg positions (031), (040), (033), (060), (020). Except for the last, these zones correspond to zones where, in the incommensurate phase, the measured satellite intensities were very strong. They are different from those selected by Currat *et al* [10], because complete deuteration of the sample modifies the elastic and inelastic structure factors. The most drastic change was observed for the (040) Bragg reflection which is very weak in the fully deuterated compound; its intensity in the incommensurate phase at 140 K is a third of the intensity of the corresponding (strong) satellite peak. The best soft branch data have in fact been obtained in the zone centred on that reflection.

(b) *The a^*–b^* plane.* In this plane we have measured low-energy modes which propagate along a^* and are mainly polarized along the b^* direction. They belong to the Σ_2 and Σ_4 irreducible representations of the wavevector group and they are degenerate at the X ($q = a^*/2$) zone boundary. The corresponding dispersion curves can also be represented in an extended zone scheme (see figure 12 later).

Constant-k_i scans were used to measure phonons in the neutron energy gain. Both the monochromator (vertically bent) and analyser (flat) were of pyrolytic graphite (PG[002]). A filter was used on k_i to avoid second-order contamination. Horizontal collimations on the incoming and scattered neutron beams were such that the instrumental energy resolution, measured on a vanadium sample, could be varied from $\Delta E = 0.25$ THz for $k_i = 2.662$ Å^{-1}, to $\Delta E = 0.015$ THz for $k_i = 1.2$ Å^{-1}.

3.3. The scattering function

The differential scattering cross section is given by

$$S(\boldsymbol{H}, \omega) = \sum_{\nu,q}^{all\ modes} S_{\nu,q}(\boldsymbol{H}, \omega) \tag{3.2}$$

where the summation is over all vibrational modes of the crystal. For one mode, one has

$$S_{\nu,q}(\boldsymbol{H}, \omega) = \langle n(\omega) + 1 \rangle |F_{in}|^2(\boldsymbol{H}) G_{\nu,q}(\omega) \delta(\boldsymbol{H} - \boldsymbol{G} \pm \boldsymbol{q}). \tag{3.3}$$

In this expression the first term is the usual Bose factor, and $F_{in}(\boldsymbol{H})$ is the inelastic structure factor:

$$F_{in}(\boldsymbol{H}) = \sum_{j=1}^{unit\ cell} m_j^{-1/2} b_j [\boldsymbol{e}_j^{\nu}(\boldsymbol{q}) \cdot \boldsymbol{H}] \exp(\mathrm{i}\boldsymbol{H} \cdot \boldsymbol{r}_j) \exp(-W_j(H)) \tag{3.4}$$

where m_j is the mass of the atom j and b_j its coherent scattering length. $W_j(H)$ is the exponent of the Debye–Waller factor and $\boldsymbol{e}_j^{\nu}(\boldsymbol{q})$ is the eigenvector of the $\nu, \boldsymbol{q}$ mode. The spectral function $G(\omega)$ was taken as a damped harmonic oscillator (DHO) response function:

$$G(\omega) = \frac{\omega \Gamma_{\nu}(\boldsymbol{q}, T)}{(\omega^2 - \omega_{\nu}^2(\boldsymbol{q}, T))^2 + \omega^2 \Gamma_{\nu}^2(\boldsymbol{q}, T)}. \tag{3.5}$$

Systematic data analysis accounting for the instrumental resolution was performed. For each value of q the data are fitted to the convolution of $S_{\nu}(\boldsymbol{H}, \omega)$ (a trial scattering function) with the resolution function of the spectrometer. The result of the fit gives for each mode the value of the three adjustable parameters:

(i) the quasi-harmonic frequency ν;
(ii) the damping constant Γ;
(iii) the norm N which is proportional to the inelastic structure factor $|F_{in}^2|$.

4. Results

The transition to the incommensurate phase has been studied previously with the Raman and infrared (IR) techniques by Ao and Schaack [16] and Volkov [17], respectively. These workers have shown that there are normal modes (at $q = 0$) which are very sensitive to temperature. More specifically, Ao and Schaack [16] have obtained two temperature-dependent optic modes assigned to symmetries B_{3g} and B_{1g}, respectively, whereas Volkov [17] has studied a B_{2u} mode which softens incompletly at T_i. As already mentioned above,

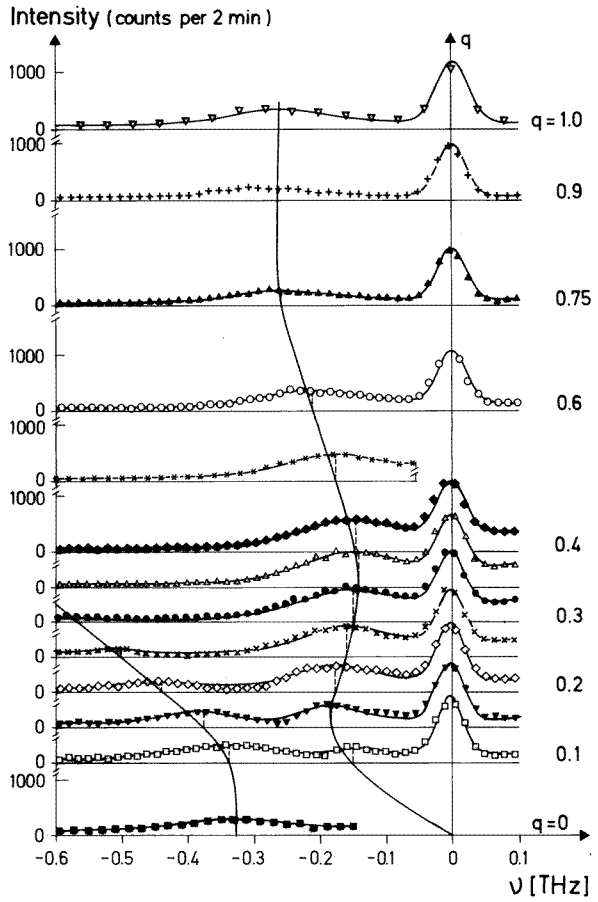

Figure 5. Constant-q scans at $(04q)$ for 205 K and for $0 < q < 1$. The full curves are the results of the DHO fits (see text).

Dvořák [15] has proposed to assign these modes to a specific librational degree of freedom of the *betaine molecule* and of the *'Ca' complex*, namely that described in the structure analysis.

We shall present here the dispersion curves of the phonon branches associated with these $q = 0$ modes, at different temperatures and in the two scattering planes mentioned above.

4.1. Modes propagating along c^*

These modes have been studied in the $(b^*–c^*)$ scattering plane.

Figure 4 shows the four lower-energy $\Lambda_2–\Lambda_3$ branches, at three temperatures (300, 205 and 171 K) in the normal phase above T_i. C_{2c}, σ_a, σ_b are the symmetry elements of the wavevector group. The Λ_3 modes are symmetric with respect to σ_a whereas the Λ_2 modes are symmetric with respect to C_{2c}. A set of constant-q scans obtained at 205 K for different q-values along c^* are displayed in figure 5.

4.1.1. $T = 300$ *K.* These are as follows.

(i) *At* $q = 0$. One measures the polar mode B_{2u} (polarized along b) and non-polar modes B_{3g}. Following Raman and IR data, the modes at 0.68 THz (22.64 cm^{-1}) and at 0.50 THz (16.65 cm^{-1}) were assigned to B_{3g} and B_{2u} symmetries, respectively. Fitted values of the damping parameter Γ have been found at 0.20($\pm$0.01) THz for the B_{2u} and 0.15($\pm$0.01) THz for the B_{3g} modes.

(ii) *At* $q = c^*$. One measures non-polar modes of B_{1g} and A_u symmetry. The modes at 0.73 THz (24.31 cm^{-1}) and 0.37 THz (12.32 cm^{-1}) have been assigned to B_{1g} and A_u symmetries, respectively. This latter mode is silent in IR and Raman measurements.

(iii) *For* $q//c^*$. The modes Λ_2–Λ_3 are mainly transverse.

(a) For small values of q ($\leqslant 0.1c^*$), when the modes do not interact, the TA mode has no intrinsic width and its slope gives a sound velocity of 1932 ms^{-1} which is only slightly smaller than that measured by Haussühl *et al* [18] the hydrogenated compound ($v = 1975$ m s^{-1}) using an ultrasonic method. Figure 6 displays such a mode measured, with the best energy resolution ($k_i = 1.20$ $Å^{-1}$), at $q = 0.05c^*$ near the very strong Bragg peak (020). The delta signal observed at $\nu = 0$ THz is due to the elastic incoherent response of our sample, whereas the sharp peak at 0.03 THz is due to Bragg contamination.

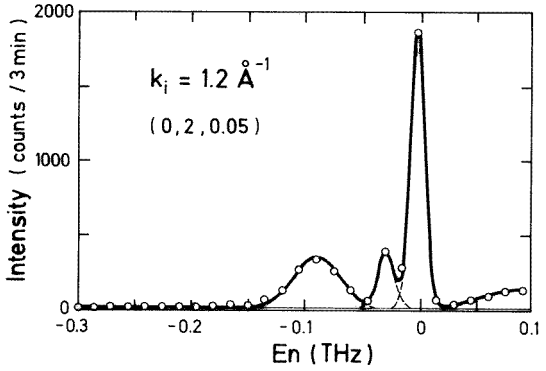

Figure 6. TA mode of symmetry Λ_3 propagating along c^* and polarized along b^*. The full line is the result of the fit including an incoherent contribution and Bragg contamination near 0.03 THz.

(b) For larger values of q, conspicuous anticrossing features are observed between the TA mode and the lowest optic mode first, and then with the second optic branch. The normal mode B_{2u} and the branch associated with it, i.e. the soft optic branch have been measured in the (040) zone. This allows measurements in a transverse configuration. The branch associated with the normal mode B_{3g} has a non-zero stucture factor in a zone centred at (033) where the configuration is intermediate between a transverse geometry and a longitudinal geometry. For $q = 0.2c^*$, where the first anticrossing between the TA mode and the first optic branch is observed, interference effects could be observed in the (040) zone. This is also seen at $T = 205$ K, and in figure 7. There the soft mode spectrum shows a sharp asymmetric profile which cannot be fitted to a sum of DHO response functions. In the same figure 7 we show the TA mode, measured in the (033) zone where the structure factor of the soft mode is very weak. This latter measurement yields the TA quasi-harmonic frequency at $q = 0.2c^*$. Interference effects were not visible for the second anticrossing, between the TA mode and the second optic branch. The profile of the constant-q scans

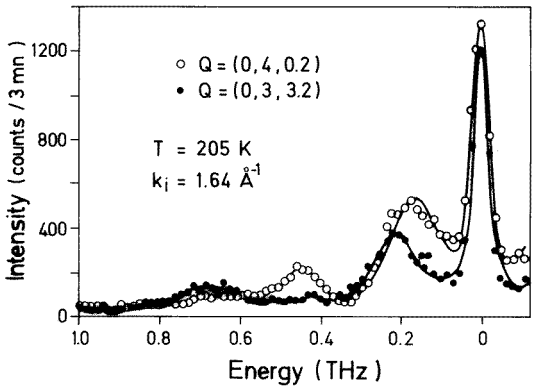

Figure 7. Energy profile scans for $T = 205$ K at $q = 0.2c^*$ in two different zones centred at (040) and (033), respectively. The full and open circles are experimental points. The full curves are the results of the fit (see text).

could be fitted by a sum of DHO response functions; the results of the fit clearly shows an interchange of the damping factors and of the structure factors between the two modes.

4.1.2. Temperature dependence. When the temperature is lowered to T_i the three lowest-energy Λ_2–Λ_3 branches are softening as seen in figure 4. The anticrossing interactions remain, but the interference effects observed at room temperature and for 205 K, disappear at lower temperatures. Therefore our data treatment, where the energy profile is fitted to the response function of a sum of independent DHOs, gives a reasonable set of parameter values ν, Γ and N for each mode.

In the following we shall be concerned with the temperature behaviour of five specific modes: the IR and Raman modes B_{2u}, B_{3g}, B_{1g} and A_u and the soft mode at $q = 0.3c^*$.

(i) *B_{2u} mode.* Figure 9 illustrates, on two constant-q scans, the softening of the B_{2u} mode. The energy profiles have been fitted to a response function which consists of DHO, for the phonon signal, a Bragg peak and a quasi-elastic peak at zero frequency. This quasi-elastic component simulates the low-frequency contamination coming from the acoustic modes collected within the finite volume of the resolution ellipsoid. The quasi-harmonic frequency ν of the mode has softened to $\nu = 0.27$ THz at 170 K. Its damping factor Γ remains nearly unchanged. Thus this mode is still underdamped a few Kelvin above T_i.

In figure 8 we have reported the frequency squared (ν^2) as a function of temperature and we show that $\nu^2 = a\ (T - T_0)$ with $a = 1.52 \times 10^{-3}$ THz^2 K^{-1}.

(ii) *The soft mode at $q = 0.3c^*$.* Figure 10 shows energy scans at $q = 0.3c^*$ for 205, 190 and 171 K. We have observed that, in the range 190–272 K, the damping constant Γ remains unchanged to 0.2 THz. Below $T = 190$ K, the soft mode becomes overdamped ($2\nu^2 < \Gamma^2$). The values of ν^2 and Γ were determined from the data, assuming as a constraint during the fit, that the structure factor N of the soft mode and of the incoherent elastic response were temperature independent. Below $T = 170$ K the energy scans at the position of the satellite exhibit a 'central peak' in addition to the inelastic response from the soft mode. On approaching T_i, the central peak strength diverges, while its frequency width appears as resolution limited (less than 15 GHz) at all temperatures. A similar central component has been observed near a wide variety of displacive structural transitions. It is believed to arise from intrinsic mechanisms. In the present case, a detailed study of its temperature and wavevector dependence was not attempted.

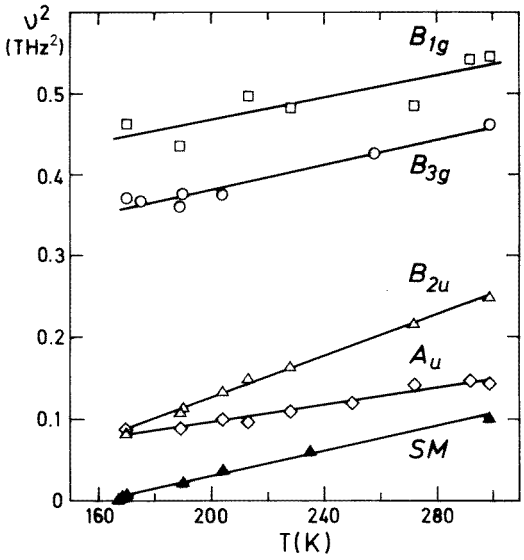

Figure 8. The dependence of ν^2 on temperature for the modes B_{2u}, A_u, B_{3g} and B_{1g} and the soft mode at $q = 0.3c^*$.

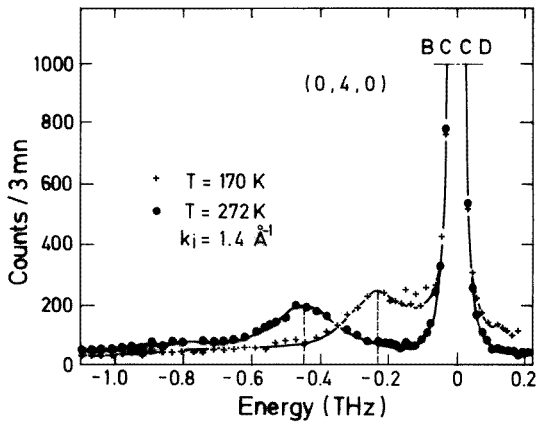

Figure 9. Constant-q scans at (040) and for $T = 170$ K and 272 K. The full curves are the results of the DHO fit.

The plot of ν^2 as a function of T reported in figure 8 obeys the Cochran law $\nu^2 = A(T - T_i)$ with $T_i = 165$ K and $A = 8 \times 10^{-4}$ THz^2 K^{-1} in agreement with the work of Currat *et al* [10].

(iii) *B_{3g}, B_{1g} and A_u modes.* For these three modes, figure 8 shows that the dependences of ν^2 on T have roughly the same linear behaviour. The slope of this line is 6×10^{-4} THz^2 K^{-1} and therefore the softening of these modes is less steep than for B_{2u} and the $q = 0.3c^*$ soft mode.

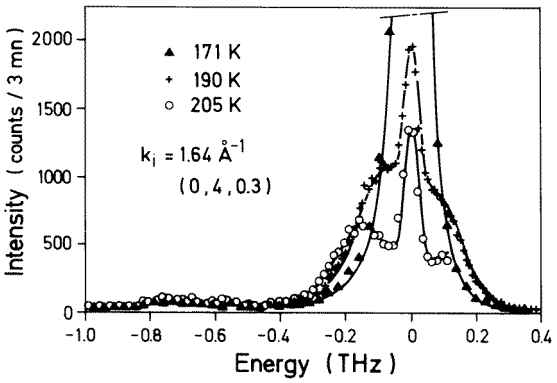

Figure 10. Constant-q scans at (040.3) and for 205, 190 and 171 K. The full curves are the results of the DHO fit.

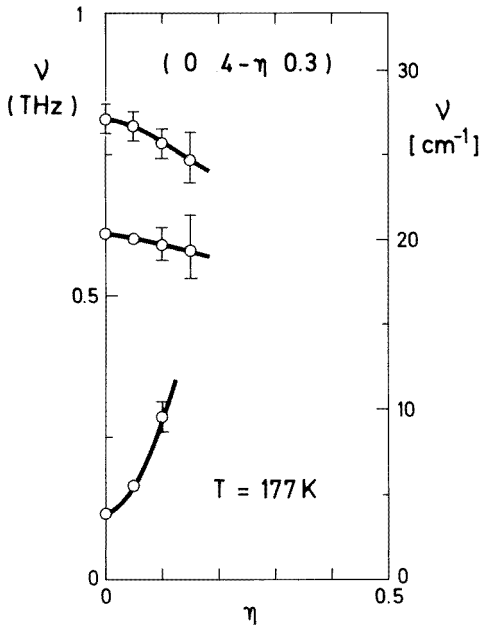

Figure 11. Dispersion of the soft branch in the b^* direction, around the frequency minimum at $q = 0.3c^*$.

4.1.3. Anisotropy of the soft branch. Finally in figure 11, we show for $T = 177$ K the renormalization of the phonon frequencies when the wavevector deviates from the c^* direction: $q = 0.3^* + \eta b^*$. This demonstrates that a large anisotropy exists for dispersion around the frequency at $q = 0.3c^*$. The b^* and c^* directions may be called the 'hard' and soft directions, respectively. This behaviour is similar to that observed for K_2SeO_4 by Iizumi *et al* [19].

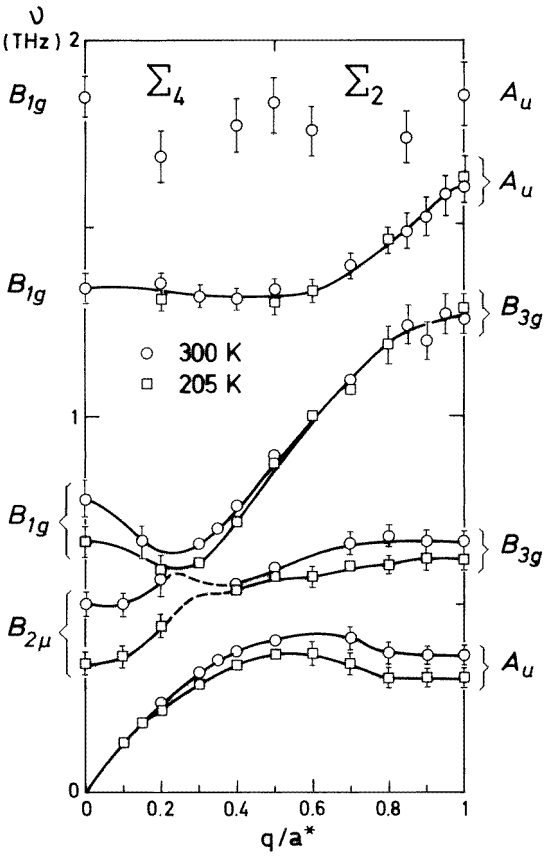

Figure 12. Σ_4–Σ_2 dispersion curves for 300 and 205 K. The full curves are guides for the eye.

*4.2. Modes propagating along a**

These modes have been measured in the (a^*–b^*) scattering plane. The symmetry elements of the group of the wavevector are C_{2a}, σ_b and σ_c. As explained before, we are interested in the modes of symmetry Σ_4 which are symmetric with respect to σ_c and with the modes Σ_2 symmetric with respect to C_{2a}. They are shown in figure 12 where the four lower-energy Σ_4–Σ_2 phonon branches are drawn in an extended zone scheme and for two temperatures.

(i) *At $q = 0$.* One measures the polar modes B_{2u} and the non-polar modes B_{1g}.
(ii) *At $q = a^*$.* One measures the modes B_{3g} and A_u.
(iii) *For q along a^*.* One obtains the Σ_4–Σ_2 dispersion curves.

The main purpose of studying these branches lies in the fact that they correspond to the low-energy $q = 0$ modes B_{2u}, B_{3g}, B_{1g} and A_u which are related to the critical degrees of freedom of the system.

As can be expected, one observes in figure 12 that the temperature behaviour in this direction has a non-critical behaviour.

5. Concluding remarks

The present experimental results show that the three lowest extended phonon branches in the a^* and c^* directions are temperature sensitive when the temperature is lowered in the normal phase of BCCD towards the incommensurate transition temperature $T_i = 164$ K. The unusual dispersion is understood as a consequence of the anticrossing of the pure acoustic branch with two bare soft optic branches. Following Dvořàk, we know that these two branches correspond to the same degree of freedom of the formula unit, namely a critical libration around an axis lying in the *m* mirror plane. Most probably the soft-mode minimum on the Λ_3 branch at $q \approx 0.32c^*$ is a consequence of this anticrossing. Qualitatively the same anticrossing scheme can be proposed for the dispersion in the a^* direction, but the softening is not critical in this direction, and no local minimum develops on the lowest branch.

Around the satellite position of the incommensurate phase, the dispersion of the soft branch has a pronounced anisotropy. All this is reminiscent of what has been observed for K_2SeO_4 by Etxebarria *et al* [20].

A more quantitative analysis of the results described above is given in the frame of a semimicroscopic model presented in the accompanying paper [21].

Acknowledgments

We are very grateful to J M Godard for growing the excellent single-crystal which has been used in this experiment. One of the authors (JH) greatly appreciated the financial support from CEA during his stay at the Laboratoire Léon Brillouin, Centre d'Etudes de Saclay.

References

[1] Brill W and Ehses K H 1985 *Japan. J. Appl. Phys.* **S-24** 826
[2] Unruh H G, Hero F and Dvořák V 1989 *Solid State Commun.* **70** 403
[3] Chaves M R, Almeida A, Toledano J C, Schneck J, Kiat J M, Schwartz W, Ribeiro J L, Müser H E, Klöpperpieper A and Albers J 1992 *Ferroelectrics* **125** 63
[4] Chaves M R, Kiat J M, Schwartz W, Schneck J, Almeida A, Klöpperpieper A, Müser H E and Albers J 1993 *Phys. Rev.* B **48** 5853
[5] Ao R, Schaack G, Schmidt M and Zöller M 1989 *Phys. Rev. Lett.* **62** 183
[6] Chaves M R, Almeida A, Kiat J M, Schwartz W, Schneck J, Toledano J C, Klöpperpieper A, Müser H E and Albers J 1992 *Phys. Rev.* B **46** 3098
[7] Chaves M R, Almeida A, Toledano J C, Schneck J, Kiat J M, Schwartz W, Ribeiro J L, Klöpperpieper A, Müser H E and Albers J 1993 *Phys. Rev.* B **46** 3098
[8] Zuniga F J, Ezpeleta J M, Pérez-Mato J M and Paciorek W 1991 *Phase Trans.* **31** 29
[9] Pérez-Mato J M 1988 *Solid State Commun.* **67** 1145
[10] Currat R, Legrand J F, Kamba S, Petzelt J, Dvořák V and Albers J 1990 *Solid State Commun.* **75** 545
[11] Brill W, Schildkamp W and Spilker J 1985 *Z. Kristallogr.* **172** 281
[12] Schildkamp W and Spilker J 1984 *Z. Kristallogr.* **168** 159
[13] Schildkamp W, Schäfer G and Spilker J 1984 *Z. Kristallogr.* **168** 187
[14] Ezpeleta J M, Zuniga J, Paulus W, Cousson A, Hlinka J and Quilichini M 1996 *Acta Crystallogr.* at press
[15] Dvořák V 1990 *Ferroelectrics* **104** 135
[16] Ao R and Schaack G 1988 *Indian J. Pure Appl. Phys.* **26** 124
[17] Volkov A A, Goncharov Yu G, Kozlov G V, Albers J and Petzelt J 1986 *JETP Lett.* **44** 603
[18] Haussühl S, Liedtke J, Albers J and Klöpperpieper A 1988 *Z. Phys.* B **70** 222
[19] Iizumi M, Axe J D, Shirane G and Shimaoka K 1977 *Phys. Rev.* B **15** 4392
[20] Etxebarria I, Quilichini M, Pérez-Mato J M, Boutrouille P, Zuniga F J and Breczewski T 1992 *J. Phys.: Condens. Matter* **4** 8551
[21] Hlinka J, Quilichini M, Currat R and Legrand J F 1996 *J. Phys.: Condens. Matter* **8** 8221–50